J. Microbiol. Biotechnol. (2009), **19**(1), 23–36
doi: 10.4014/jmb.0803.213
First published online 23 October 2008

JOURNAL OF MICROBIOLOGY AND BIOTECHNOLOGY

Investigation of the Central Carbon Metabolism of *Sorangium cellulosum*: Metabolic Network Reconstruction and Quantification of Pathway Fluxes

Bolten, Christoph J.[1], Elmar Heinzle[1], Rolf Müller[2], and Christoph Wittmann[1,†]*

[1]*Biochemical Engineering, Saarland University, D-66041 Saarbrücken, Germany*
[2]*Pharmaceutical Biotechnology, Saarland University, D-66041 Saarbrücken, Germany*

Received: March 18, 2008 / Accepted: June 13, 2008

In the present work, the metabolic network of primary metabolism of the slow-growing myxobacterium *Sorangium cellulosum* was reconstructed from the annotated genome sequence of the type strain So ce56. During growth on glucose as the carbon source and asparagine as the nitrogen source, So ce56 showed a very low growth rate of 0.23 d^{-1}, equivalent to a doubling time of 3 days. Based on a complete stoichiometric and isotopomer model of the central metabolism, ^{13}C metabolic flux analysis was carried out for growth with glucose as carbon and asparagine as nitrogen sources. Normalized to the uptake flux for glucose (100%), cells recruited glycolysis (51%) and the pentose phosphate pathway (48%) as major catabolic pathways. The Entner-Doudoroff pathway and glyoxylate shunt were not active. A high flux through the TCA cycle (118%) enabled a strong formation of ATP, but cells revealed a rather low yield for biomass. Inspection of fluxes linked to energy metabolism revealed that *S. cellulosum* utilized only 10% of the ATP formed for growth, whereas 90% is required for maintenance. This explains the apparent discrepancy between the relatively low biomass yield and the high flux through the energy-delivering TCA cycle. The total flux of NADPH supply (216%) was higher than the demand for anabolism (156%), indicating additional reactions for balancing of NADPH. The cells further exhibited a highly active metabolic cycle, interconverting C_3 and C_4 metabolites of glycolysis and the TCA cycle. The present work provides the first insight into fluxes of the primary metabolism of myxobacteria, especially for future investigation on the supply of cofactors, building blocks, and energy in myxobacteria, producing natural compounds of biotechnological interest.

Keywords: Myxobacteria, primary metabolism, flux, NADPH, maintenance

*Corresponding author
Phone: 49-0-531-391-7661; Fax: 49-0-531-391-7652
E-mail: c.wittmann@.tu-bs.de

†Present address: Christoph Wittmann, Biochemical Engineering Institute, Technische Universität Braunschweig, Gaussstrasse 17, D-38106 Braunschweig, Germany

Myxobacteria have remarkable properties such the ability to glide on solid surface, form fruiting bodies and biofilms, and live as micropredators [13]. Additionally, they exhibit an outstanding biotechnological potential as sources for the production of natural compounds [13, 30, 31]. One of the most relevant species in the taxon of myxobacteria is *Sorangium cellulosum*. Screening of various myxobacterial species revealed that almost 50% of all newly discovered natural products are produced by *S. cellulosum* [13]. Hereby, *S. cellulosum* strains typically form a number of different compounds that sometimes are structurally related [16], but can also be chemically rather different [18–21]. Various secondary metabolites from *S. cellulosum* such as epothilone [11], ratjadon [14], sorangicin [20], or soraphen [12] are of high biotechnological interest. Among all these compounds, epothilone, which possesses taxol-like antitumor activity, is the most promising one [6, 7, 36]. The fascinating properties of myxobacteria and the high economical interest in their products have stimulated intensive research on these organisms in recent years. From the metabolic viewpoint, research has focused mainly on the secondary metabolism leading to the identification of novel products and the study of the underlying assembling pathways [4, 13]. In contrast, the primary metabolism has been studied only to a limited extent. Pathways of the primary metabolism, however, display a key role in myxobacteria since they supply the precursors of secondary metabolites, such as acetyl CoA as the building block of polyketide chains or amino acids. It is therefore obvious that studies on the functioning and regulation of primary metabolic routes will significantly contribute to the understanding of the formation of natural products in myxobacteria. This is highlighted by recent identification of novel pathways for fatty acid [25] or steroid [5] biosynthesis in myxobacteria.

An excellent approach in this context is ^{13}C metabolic flux analysis, which allows the precise and detailed quantification of carbon fluxes through central metabolic pathways, as recently demonstrated for different prokaryotes and eukaryotes [9, 10, 15, 42], but no knowledge is available so far on metabolic fluxes in myxobacteria.

The present work describes the reconstruction of the metabolic network of *S. cellulosum* comprising catabolic and anabolic pathways of the primary carbon metabolism from the recently sequenced genome of *S. cellulosum* So ce56 [34]. Based on this and a detailed analysis of cellular composition, a mathematical model involving stoichiometric and isotopomer balancing was set up and applied to study carbon fluxes in So ce56 through combination with ^{13}C tracer experiments and GC/MS labeling analysis of metabolites, providing the first insight into *in vivo* activities of enzymes and pathways of the primary metabolism for members of the myxobacterial group.

Material and Methods

Strains

S. cellulosum 56 (So ce56), studied in the present work, is regarded as the model organism of the genus *Sorangium* [13, 29]. It has been completely sequenced [34]. Its repertoire of enzymes and pathways is available in the KEGG database (http://www.genome.jp/kegg/).

Media and Cultivation

Sorangium cells were grown on agar plates with complex medium containing, per liter, 0.2% peptone, 0.5% starch, 0.2% glucose, 0.1% probion, 0.05% $MgSO_4 \cdot 7H_2O$, 0.05% $CaCl_2 \cdot 2H_2O$, 1.2% HEPES, and 1.4% agar. The medium was adjusted to pH 7.6 and subsequently autoclaved. Cells grown on the plates at 30°C for five days served as inoculum for precultures, which were grown in 100-ml shake flasks with 10 ml of defined *Sorangium*-zinc (SG-Zn) medium for five days. Afterwards, cells were harvested and used as inoculum of main cultures grown in 250-ml shake flasks with 50 ml of SG-Zn medium. Cultivation supernatant for quantification of substrates and products was obtained during the cultivation by centrifugation (5 min, room temperature, 16.000 ×*g*; Biofuge fresco; Kendro Laboratory Products, Langenselbold, Germany). All shake flask cultivations were carried out at 30°C and 230 rpm on a rotary shaker (shaking diameter Ø 50 mm; Multitron II; Infors AG, Bottmingen-Basel, Switzerland). The SG-Zn medium contained, per liter, 0.05% $MgSO_4 \cdot 7H_2O$ and 2.4% HEPES (dissolved in deionized water, adjusted to pH 7.2 and then autoclaved), amended with separately autoclaved stock solutions to final concentration of 1.0% glucose, 0.05% $CaCl_2 \cdot 2H_2O$, 0.001% Fe-EDTA, 0.001% $ZnSO_4 \cdot 7H_2O$, and 0.006% K_2HPO_4. Additionally, filter-sterilized asparagine·H_2O was added to a final concentration of 0.35%. In labeling studies, naturally labeled glucose was replaced by an equimolar concentration of 99% [1-^{13}C] glucose (Cambridge Isotope Laboratories, Andover, U.S.A.).

Chemicals

Complex substrates were obtained from Difco Laboratories (Detroit, MI, U.S.A.). All other chemicals were from Sigma (Steinheim, Germany) or Merck (Darmstadt, Germany) and of analytical grade.

Analysis of Cell and Glucose Concentration

The concentration of cells was measured *via* optical density at 600 nm ($OD_{600\ nm}$) using a photometer (Spectrophotometer Ultrospec; Pharmacia Biotech, Little Chalfont, U.K.) or by gravimetry. The correlation factor between cell dry weight (CDW) and $OD_{600\ nm}$ was determined as 0.308 (g CDW/OD unit). The dissolved oxygen concentration in shake flask cultivations was measured *via* immobilized fluorescence sensors on the flask bottom and the optical system OXY-4 (PreSens Precision Sensing GMBH, Regensburg, Germany) as described previously [47]. Glucose in the culture supernatant was quantified by HPLC (Kroma System; Kontron Instruments, Biotek, Neufahrn, Germany), utilizing an Aminex-HPX-87H Bio-Rad column (300×7.8 mm; Hercules, CA, U.S.A.) with 7 mM H_2SO_4 as the mobile phase at a flow rate of 1.0 ml/min [2].

Labeling Analysis

The labeling pattern of amino acids (from hydrolyzed and lyophilized cell protein) and trehalose (from lyophilized cultivation supernatant) was quantified by GC/MS (HP 6890, Quadrupol Mass Selective Detector 5973; Agilent Technologies, Waldbronn, Germany). The hydrolysis of the cell protein followed a protocol previously described [41]. Amino acids were analyzed as t-butyldimethylsilyl derivates [41]. Trehalose was measured as trimethylsilyl derivate [46]. All samples were measured first in scan mode, therewith excluding isobaric interference between analyzed products and other sample components. The relative fractions of different mass isotopomers (M_0, M_1,..) were then determined in triplicate in selective ion monitoring (SIM) mode.

Analysis of Cellular Composition

Cells of *S. cellulosum* So ce56 were harvested during exponential growth by centrifugation (5 min, room temperature, 16.000 ×*g*; Biofuge fresco; Kendro Laboratory Products, Langenselbold, Germany). The protein content was quantified based on a protocol of Lowry *et al.* [24]. In detail, protein extraction was performed by incubating cells for 10 min in 0.64 N NaOH at 100°C. After separation of cell debris by centrifugation (10 min, room temperature, 800 ×*g*; Labfuge 400R; Heraeus/Kendro, Osterode, Germany), 1.5 ml of supernatant was mixed with 1.5 ml of reagent solution (1.16 M Na_2CO_3, 6 mM Na-K-tartrate·$4H_2O$, 2 mM $CuSO_4 \cdot 5H_2O$), and incubated for 10 min at room temperature. Subsequently, Folin-Ciocalteus reagent was added. After 30 min incubation at room temperature, the extinction was measured photometrically at 625 nm (Spectrophotometer Ultrospec; Pharmacia Biotech, Little Chalfont, U.K.). Protein quantification was carried out *via* external calibration using bovine serum albumin as the standard. The amino acid composition of the cell protein was measured after cell hydrolysis (6 M HCl, 24 h, 105°C) by HPLC as described previously [22]. Lipid extraction and quantification was done as given by Bligh and Dyer [3]. The composition of the lipid fraction was analyzed as described by Minnikin *et al.* [26]. DNA was extracted using a commercial kit (Purgene DNA Purification Kit for Gram-negative Bacteria Culture; Gentra Systems, Minnesota, U.S.A.). DNA concentration was quantified *via* extinction measurement at 260 nm (Biophotometer; Eppendorf, Hamburg, Germany). In the case of DNA, the demand for nucleotides was estimated from the GC content (71.4 %) of the So ce56 genome. RNA was extracted by addition of 750 µl of TRIzol (QIAzol Lysis Reagent; QIAGEN, Hilden, Germany) to the cell pellet. The solution was heated up to 50°C and then centrifuged for 10 min at 16.000 ×*g* and 4°C (Biofuge

fresco; Kendro Laboratory Products, Langenselbold, Germany). The supernatant was mixed with 150 µl of $CHCl_3$ and incubated for 3 min at room temperature. The two phases were separated by centrifugation (15 min, 14.800 ×*g* 4°C; Biofuge fresco; Kendro Laboratory Products, Langenselbold, Germany). The upper aqueous phase was mixed with 190 µl of isopropanol and 190 µl of salt solution (0.8 M Na-citrate, 1.2 M NaCl) and then incubated for 10 min at room temperature. After centrifugation (10 min, 11.500 ×*g*, 4°C; Biofuge fresco; Kendro Laboratory Products, Langenselbold, Germany), the sedimented RNA was washed with 75% ethanol and resuspended in 50 µl of water. After 1:100-fold dilution with TE-buffer (10 mM Tris/HCl, 1 mM EDTA; pH 8.0), the RNA concentration was measured photometrically at 260 nm (Biophotometer; Eppendorf, Hamburg, Germany). The nucleotide composition of RNA was calculated from the sequence of the genes for rRNA, assuming that the RNA pool is only composed of rRNA.

Metabolic Modeling and Calculation of Metabolic Fluxes

The reconstructed metabolic network of the central metabolism of *S. cellulosum* (see Appendix) was implemented into a computer model in the mathematical software platform Matlab 7.0 (Mathworks Inc., Nattick, U.S.A.). All simulations were carried out on a personal computer. The computer model is a condensed representation of the entire metabolic network. Details on the network are given in the Appendix. A metabolite pool for CO_2 was implemented, reflecting its mass isotopomer distribution as a result of the CO_2 producing and consuming reactions in the network. The incorporation of non-labeled CO_2 from ambient air was accounted for as described previously [23]. The computer model comprised metabolite and isotopomer balancing around intracellular metabolite pools. For a given set of fluxes, it computes the labeling pattern of the network metabolites, including different amino acids. Hereby, the simulated labeling data are converted into mass isotopomer distributions of corresponding ion fragments accessible *via* GC-MS analysis from the tracer experiments. This involves the correction for natural isotopes [37, 43]. The mass isotopomer fractions are highly sensitive to changes in intracellular fluxes. Like a fingerprint, these data reflect the intracellular fluxes and can thus effectively be used for their estimation. Starting from random numbers for the free fluxes, the employed metabolic model calculates the remaining dependent fluxes *via* the mass balances and subsequently computes the ^{13}C labeling patterns. An implemented algorithm then minimizes the deviation between experimental and simulated mass isotopomer fractions by variation of the free fluxes. The set of fluxes with minimum deviation between experimental and simulated data is then taken as best estimate for the intracellular flux distribution. Further details on the applied computational tools are given elsewhere [42, 44, 45]. In the present work, 38 mass isotopomer fractions were considered as experimental data. The network was overdetermined, so that a least-square approach was possible (see Appendix). As error criterion, a weighed sum of least squares was used. Identical flux distributions were obtained with multiple randomized initialization values, showing that a global minimum was identified. Statistical analysis of the obtained fluxes was carried out by a Monte-Carlo approach [42]. The statistical variation was done such that random errors were added to the data sets, assuming a normal distribution of measurement errors around previously obtained mean values. The normally distributed random errors were generated using the statistics toolbox of Matlab. The errors considered were the measurement errors of the MS analysis and the stoichiometric data from the tracer studies. By this approach, the statistical analysis yields information on the accuracy and confidence directly related to the performed corresponding tracer experiments. Subsequently, 100 independent parameter estimations were carried out, yielding 100 flux distributions with a corresponding mean value and a standard deviation for each intracellular flux parameter, from which 90% confidence limits for the single parameters were calculated.

RESULTS

Metabolic Network of *S. cellulosum*

The primary carbon metabolism of *Sorangium cellulosum,* studied in the present work comprises several hundred metabolic reactions. The organism possesses different catabolic pathways (*i.e.*, glycolysis, pentose phosphate pathway (PPP), Entner-Doudoroff pathway (EDP), and TCA cycle) for the metabolization of glucose. It is interesting to note that the organism has a large repertoire of anaplerotic reactions including pyruvate carboxylase, phosphoenolpyruvate carboxylase, phosphoenolpyruvate carboxykinase, malic enzyme, and the glyoxylate shunt enzymes isocitrate lyase and malate synthase. On the basis of the anabolic pathways present, the exact stoichiometric demand for precursors and cofactors for biosynthesis of each of the biomass constituents was derived (Table 1). The complete set of pathways was implemented into a metabolic model of the primary metabolism comprising metabolite and isotopomer balancing that was utilized for the quantification of metabolic fluxes. The underlying reconstructed metabolic network of *Sorangium cellulosum* is displayed in Fig. 1. It is a condensed representation of about 300 reactions in the catabolism and anabolism of the organism, carrying substantial carbon flux during growth on glucose and asparagine. The condensation comprises the lumping of subsequent reaction steps in linear pathways and of pathways at the network periphery (*e.g.* towards anabolism) into single reactions.

Cultivation Profile

The cultivation profile of So ce56 on defined medium with glucose and asparagine as substrates is displayed in Fig. 2. During the first 20 days, the strain grew exponentially with a specific growth rate of 0.23 d^{-1}. Growth was coupled to simultaneous consumption of glucose and asparagine. Neither aspartate nor oxaloacetate accumulated in the medium. Obviously, asparagine was completely metabolized and served as both carbon and nitrogen sources. During this phase, the specific substrate rates were 2.50 mmol/g/d (glucose) and 0.65 mmol/g/d (asparagine). After 21 days So ce56 reached a cell concentration of almost 2 g CDW/l. Then the growth stopped and cells entered into a stationary phase for a further 12 days. At this time point, limitation of dissolved oxygen, glucose, or asparagine or extreme pH

Table 1. Anabolic precursor demand for biomass synthesis in *S. cellulosum* So ce56 in μmol/g dry cell mass.

Precursor	Demand (μmol/g)	G6P	F6P	R5P	E4P	GAP	PGA	PEP	PYR	AcCoA	OAA	AKG	NADPH
Alanine	548								1				1
Arginine	243											1	4
Asparagine/Aspartate	483										1		1
Cysteine	78						1						5
Glutamine/Glutamate	503											1	1
Glycine	598						1						1
Histidine	74			1									1
Isoleucine	137								1		1		5
Leucine	364								2	1			2
Lysine	201								1		1		4
Methionine	131										1		8
Phenylalanine	133				1			2					2
Proline	206											1	3
Serine	244						1						1
Threonine	229										1		3
Tryptophan	48			1	1			1					2
Tyrosine	87				1			2					2
Valine	240								2				2
Protein		**0**	**0**	**122**	**269**	**0**	**920**	**489**	**2,094**	**364**	**1,181**	**952**	**9,398**
ATP	32			1			1						1
GTP	43			1			1						
CTP	57			1							1		1
UTP	44			1							1		1
RNA		**0**	**0**	**175**	**0**	**0**	**75**	**0**	**0**	**0**	**101**	**0**	**133**
dATP	10			1			1						2
dGTP	25			1			1						1
dCTP	25			1							1		2
dTTP	10			1							1		3
DNA		**0**	**0**	**71**	**0**	**0**	**36**	**0**	**0**	**0**	**36**	**0**	**127**
Glycerol 3-Phosphate	429					1							1
Serine	429						1						1
11-Methyldodecanoic (0.1 %)									2	5			10
Tetradecanoic (1.2%)										7			12
13-Methyldodecanoic (13.0%)									2	6			12
Hexadecanoic (19.3%)										8			14
11(Z)-Hexadecenoic (39.7%)										8			13
Hexadecandienoic (0.04%)										8			12
2-Hydroxyhexadecanoic (0.2%)										8			14
3-Hydroxyhexadecanoic (0.1%)										8			14
15-Methylhexadecanoic (16.9%)									2	7			14
15-Methylhexadecenoic (1.0%)									2	7			13
2-Hydroxy-15-methylhexadecanoic (0.3%)									2	7			14
3-Hydroxy-15-methylhexadecanoic (0.7%)									2	7			14
Octadecanoic (7.4%)										9			18
Average Fatty acids	*858*								*0.6*	*7.6*			*13.6*
Lipids						**429**	**429**		**548**	**6,530**			**12,528**

can all be excluded as reasons for the cease of cell growth. During the stationary phase, cells consumed the residual glucose and asparagine, whereby the relative uptake of asparagine among the two substrates was enhanced. With the complete depletion of glucose and asparagine after 35 days the cell concentration decreased. The biomass yield during the exponential growth phase was 0.0537 g CDW/mmol glucose and thus rather low. Production of

Table 1. Continued.

Precursor	Demand (μmol/g)	G6P	F6P	R5P	E4P	GAP	PGA	PEP	PYR	AcCoA	OAA	AKG	NADPH
UDP Glucose	24	1											
(CDP) Ethanolamine	36						1						1
OH-Mystric acid	36									7			11
C14:0	36									7			12
(CMP) KDO	36			1				1					
(NDP) Heptose	36	1.5											-4
(TDP) Glucosamine	24		1										
LPS		**78**	**24**	**36**	**0**	**0**	**36**	**36**	**0**	**504**	**0**	**0**	**720**
UDP-N-Acetylglucosamine	43		1							1			
UDP-N-Acetylmuramic acid	43		1					1		1			1
Alanine	85								1				1
Diaminopimelate	43								1		1		4
Glutamate	43											1	1
Peptidoglycan		**0**	**86**	**0**	**0**	**0**	**0**	**43**	**128**	**86**	**43**	**43**	**343**
Glucose	238	1											
Glycogen		**238**											
Serine	49						1						1
C_1-units							**49**						**49**
Ornithine equivalents	59											1	3
Polyamines												**59**	**177**
Total		**316**	**109**	**405**	**269**	**429**	**1,544**	**568**	**2,770**	**7,486**	**1,360**	**1,054**	**23,478**

secondary metabolites was not detected. Moreover, by-products of primary metabolism such as organic acids were not formed. Biomass and CO_2 were the sole major products under the conditions tested. So ce56 did not grow when aspartate instead of asparagine was used as the nitrogen source, but could utilize ammonium sulfate as the sole source of nitrogen (data not shown). The relative fractions of cellular polymers in So ce56 (*i.e.*, protein, lipids, RNA, DNA, and carbohydrates) are shown in Table 2. The macromolecular composition was further broken down into the cellular content of single building blocks for each macromolecular fraction. Via the anabolic pathways identified, the exact demand of all anabolic precursors (*i.e.*, the anabolic pathway fluxes) during growth of So ce56 was determined (Table 1).

Metabolic Pathway Fluxes

It was now interesting to see how the different pathways of the central metabolism contributed to the overall metabolic activity of *S. cellulosum*. As an example, the high lipid content posed an enormous demand for NADPH to the organism, raising the question for NADPH-supplying pathways. For this purpose, intracellular fluxes were quantified on the basis of tracer cultivations with [1-^{13}C] glucose and nonlabeled asparagine and a rich set of labeling (Table 3) as well as stoichiometric (Table 1, Table 2) data. The intracellular flux distribution obtained for So ce56 is shown in Fig. 3. Glucose and asparagine were both taken up simultaneously, whereby about 80% of substrate molecules utilized were represented by glucose. Glycolysis and PPP were utilized for glucose metabolization, whereas the EDP was inactive. The flux into the PPP (48.0%) was much higher than the demand for the anabolic precursor ribose 5-phosphate (2.2%) and erythrose 4-phosphate (1.4%) and significantly contributed to the supply of NADPH. The high PPP flux resulted in a significant back-flux of carbon from the PPP to the pools of F6P and GAP in the glycolytic chain. Reactions catalyzed by glucose 6-phosphate isomerase, transketolase, and transaldolase exhibited significant reversibility. So ce56 revealed high flux through carboxylating and decarboxylating reactions connecting the TCA cycle and glycolysis. The flux through carboxylating anaplerotic enzymes (pyruvate carboxylase, phosphoenolpyruvate carboxylase) was lower than that through the gluconeogenic enzymes (phosphoenolpyruvate carboxykinase, malic enzyme), so that overall a net flux from the TCA cycle towards the glycolysis resulted. On the basis of the labeling data, these fluxes can be given only as a lumped value of the different enzymes potentially involved. It is however clear that So ce56 exhibited a highly active metabolic cycle, interconverting C_4 and C_3 metabolites of glycolysis and the TCA cycle. The activity of this cycle (40%) was about 4-fold higher than the corresponding net flux. The glyoxylate pathway in So ce56 was not active. With regard to the anabolic pathways,

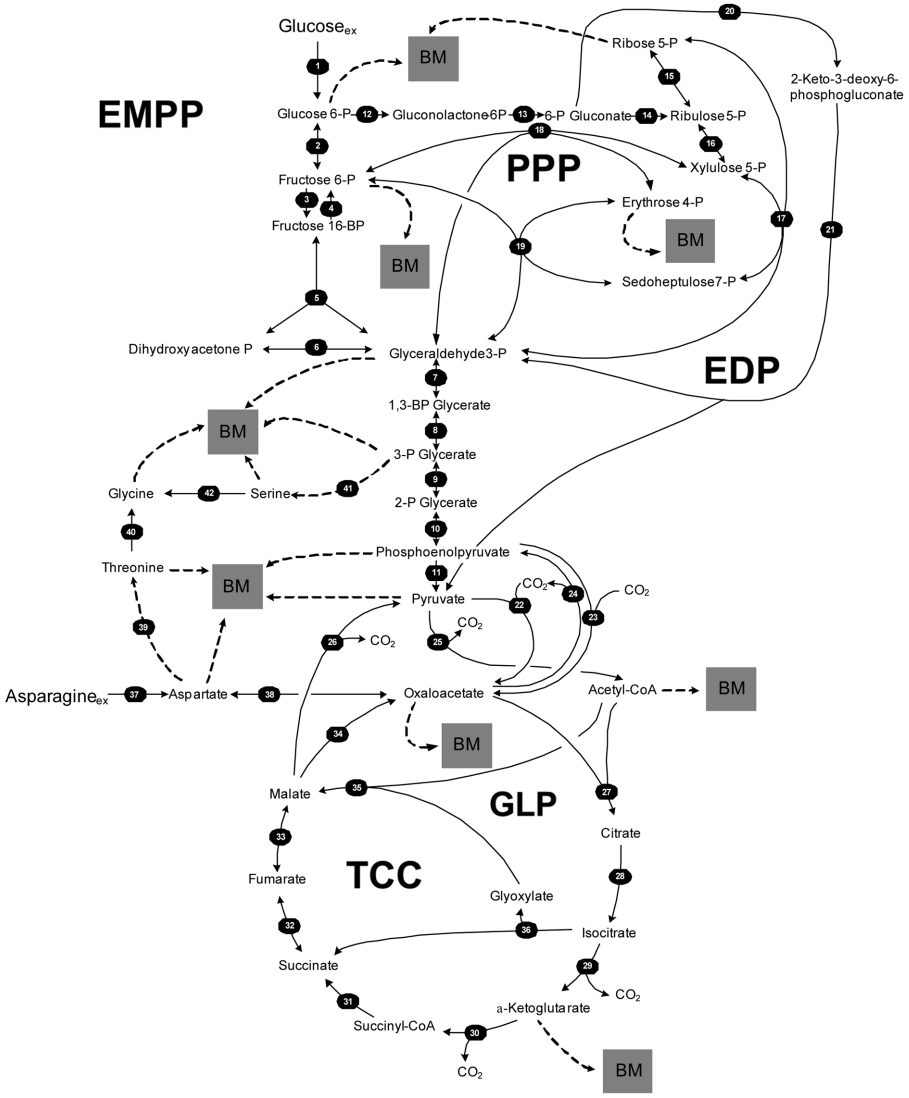

Fig. 1. Metabolic network of the primary carbon metabolism of *Sorangium cellulosum* So ce56 including transport, catabolic, and anabolic reactions.

EMPP, Emden-Meyerhof-Parnas pathway (glycolysis); PPP, pentose phosphate pathway; EDP, Entner-Doudoroff pathway; GLP, glyoxylate pathway; TCC, tricarboxylic acid cycle. It should be noted that all pathways at the network periphery (*e.g.*, towards anabolism) are shown here as lumped single reactions to facilitate the graphical representation of the network.

one should note the enormous flux from acetyl-CoA towards anabolism (40%), mainly for the formation of fatty acids (Table 1). The major fraction of asparagine was channeled *via* aspartate into the TCA cycle. The simultaneous influx from asparagine into the oxaloacetate pool and from glucose into the citrate pool resulted in a remarkably high TCA cycle flux enabling efficient generation of reduction equivalents for energy supply. Carbon from the glucose skeleton was utilized for the synthesis of aspartate-derived biomass constituents such as threonine. This is directly reflected by the increased fractions of higher labeled mass isotopomers in these compounds, which obviously did not originate from the unlabeled asparagine (Table 3) and indicates a highly reversible transamination reaction between aspartate and oxaloacetate, which was confirmed by the flux calculation. Interestingly, the effective supply of the aspartate pool *via* the uptake of asparagine triggered an alternative pathway for the formation of glycine. In addition to the normal route from serine, threonine aldolase, catalyzing the cleavage of threonine into acetaldehyde and glycine, was found to be active. This second pathway even supplied the major fraction of glycine. Experimental and simulated values corresponding to the optimal fit of fluxes showed excellent accordance (Table 3), so that the metabolic network of *S. cellulosum* described the experimental data very well.

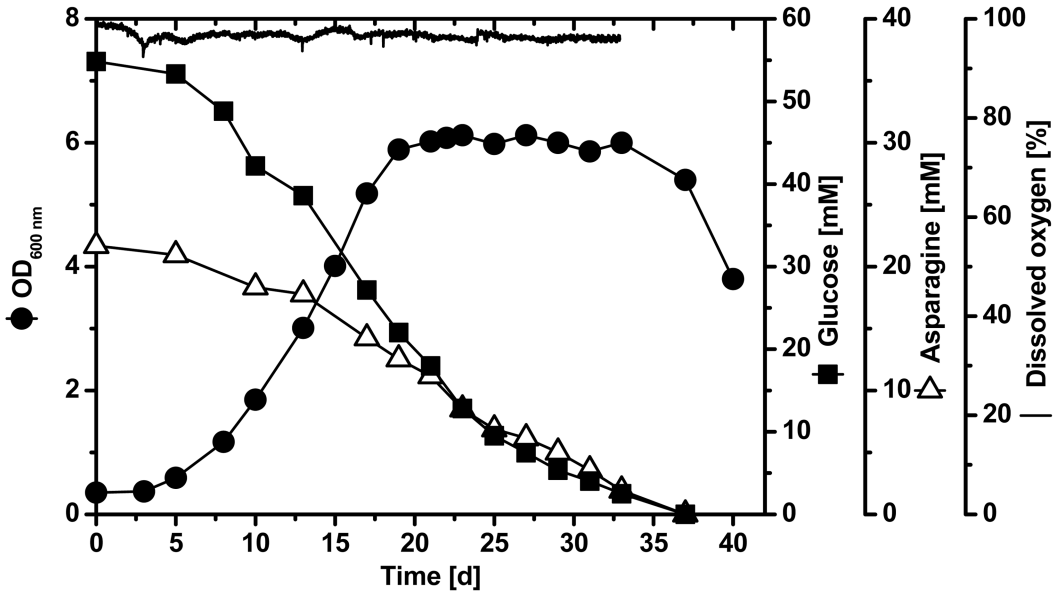

Fig. 2. Cultivation profile of *Sorangium cellulosum* So ce56 on defined medium with glucose and asparagine as sources of carbon and nitrogen: concentrations of glucose, asparagine, cell concentration (optical density), and dissolved oxygen.

DISCUSSION

Metabolic Network

The reconstructed metabolic network of the primary carbon metabolism of So ce56 illustrates that this organism comprises a rich repertoire of catabolic pathways. Owing to the excellent fit of the data, we conclude that the assembled metabolic network of *S. cellulosum* indeed contains all relevant pathways of this organism during growth on glucose and asparagine.

Catabolic Pathways

The present work shows that the PPP plays a much more important role in the metabolism of *S. cellulosum*, as previously suggested. About 50% of glucose is channeled into the PPP. A previous study utilizing radioactive tracer substrates suggested that the PPP flux for glucose-grown *S. cellulosum* is almost insignificant [17]. This study, however, neglected important features of the studied network, required for precise quantification of the PPP

Table 2. Macromolecular composition of *S. cellulosum* So ce56.

Compound	Content (g/g CDW)
Protein	0.48
Carbohydrates	0.12
RNA	0.06
DNA	0.02
Lipids	0.30
Ash	0.02

Data on the carbohydrate content are taken from the literature [1].

Table 3. Relative mass isotopomer fractions of amino acids from the cell protein and of secreted trehalose of *S. cellulosum* 56 cultivated on 99% [1-^{13}C] glucose and nonlabeled asparagine.

Amino acid		Mass isotopomers			
		M_0	M_1	M_2	M_3
Alanine (*m/z* 260)	Calc	0.501	0.349	0.117	
	Exp	0.506	0.348	0.115	
Valine (*m/z* 288)	Calc	0.338	0.390	0.192	
	Exp	0.337	0.391	0.193	
Threonine (*m/z* 404)	Calc	0.405	0.334	0.177	
	Exp	0.405	0.333	0.177	
Arginine (*m/z* 442)	Calc	0.260	0.356	0.233	0.104
	Exp	0.262	0.352	0.233	0.105
Glutamate (*m/z* 432)	Calc	0.278	0.361	0.225	0.096
	Exp	0.280	0.363	0.224	0.094
Serine (*m/z* 390)	Calc	0.441	0.356	0.151	
	Exp	0.442	0.353	0.153	
Phenylalanine (*m/z* 336)	Calc	0.223	0.357	0.256	0.115
	Exp	0.224	0.353	0.256	0.116
Glycine (*m/z* 246)	Calc	0.647	0.263		
	Exp	0.651	0.263		
Tyrosine (*m/z* 466)	Calc	0.192	0.330	0.264	0.138
	Exp	0.193	0.323	0.266	0.141
Lysine (*m/z* 431)	Calc	0.277	0.353	0.225	0.100
	Exp	0.279	0.347	0.227	0.102
Trehalose (*m/z* 361)	Calc	0.105	0.481	0.257	0.113
	Exp	0.105	0.486	0.256	0.110

Data shown are experimental GC-MS data (exp) and values predicted by the solution of the mathematical model corresponding to the optimized set of fluxes (calc). Amino acids were analyzed by GC-MS as *t*-butyldimethylsilyl derivates and trehalose as trimethylsilyl derivate, respectively.

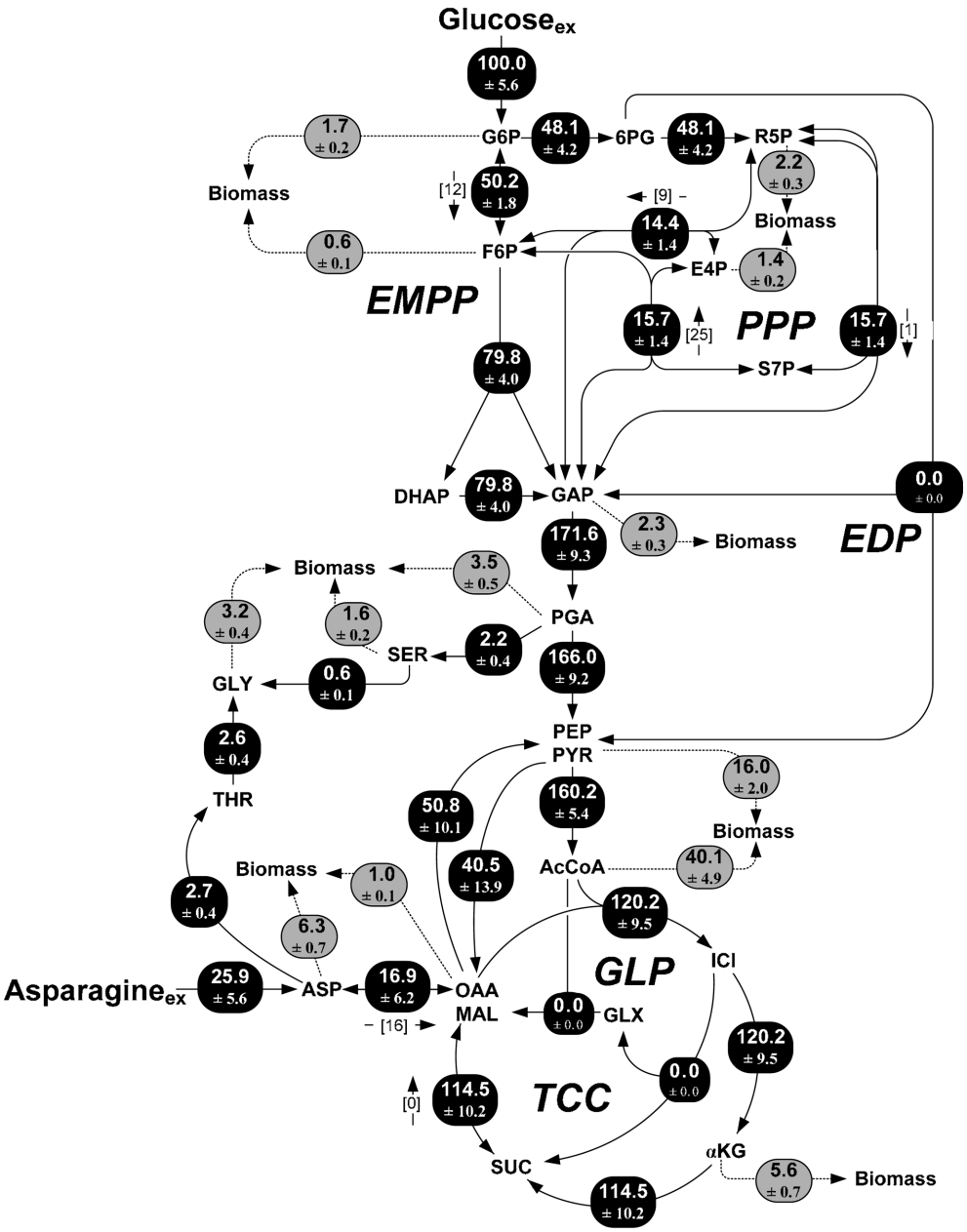

Fig. 3. *In vivo* carbon flux distribution in the central metabolism of *Sorangium cellulosum* So ce56 during growth on glucose and asparagine.

The fluxes were estimated from the best fit of GC-MS labeling data of amino acids from the cell protein and secreted trehalose from cultivation with [1-^{13}C] glucose and nonlabeled asparagine, using a comprehensive approach of combined metabolite balancing and isotopomer. For reversible reactions, the direction of the net flux is indicated by an additional arrow aside the corresponding reaction. Numbers in brackets indicate flux reversibilities. All fluxes are expressed as a molar percentage of the specific glucose uptake rate (2.5 mmol/g/d).

flux and considered in the present work (*i.e.*, bidirectional and reversible reactions or fixation of labeled CO_2) [39]. The strong activity of the PPP is probably related to the high anabolic NADPH demand (Table 1), but seems also crucial for synthesis of secondary metabolites, typically demanding for this cofactor. Because of the concerted action of carboxylating and decarboxylating enzymes around the pyruvate node, a highly active metabolic cycle, interconverting C_4 and C_3 metabolites of glycolysis and the TCA cycle, was present. The activity of this cycle (40%) was about 4-fold higher than the corresponding net flux (10–11%). Similar metabolic cycles have been shown for other bacteria including *E. coli*, *B. subtilis*, or *C. glutamicum*, where they are supposed to be involved in

Table 4. Biochemical reactions of the primary carbon metabolism of *Sorangium cellulosum* So ce56.

Reaction number	Gene product	Gene number	Gene name
Glycolysis/gluconeogenesis			
1	Hexokinase	sce6033	*hxk*
2	G6P isomerase	sce5669	*pgi*
3	6-Phosphofructokinase	sce5865	*pfk*
4	Fructose bisphosphatase	sce2578	*fbp2*
		sce8557	*glpX*
5	Fructose bisphosphate aldolase	sce2579	*fba2*
		sce1923	*fba1*
6	Triose phosphate isomerase	sce7348	*tpi*
7	GAP dehydrogenase	sce7350	*gap*
8	Phosphoglycerate kinase	sce7349	*pgk*
9	Phosphoglycerate mutase	sce1044	*pgm1*
		sce4502	*pgm2*
10	Enolase	sce7698	*eno*
11	Pyruvate kinase	sce4540	*pyk*
Pentose phosphate pathway			
12	G6P dehydrogenase	sce4355	*zwf1*
		sce7012	*zwf2*
13	6-Phosphogluconolactonase	sce4353	*pgl*
14	6-Phosphogluconate dehydrogenase	sce3546	*gnd1*
		sce6035	*gnd2*
15	Ribose 5-phosphate isomerase	sce1758	*rpiA*
16	Ribulose 5-phosphate 3-epimerase	sce8198	*rpe*
17	Transketolase 1	sce3987	*tkt1*
18	Transketolase 2	sce8467	*tkt2*
19	Transaldolase	sce1460	*tal1*
		sce0029	*tal2*
Entner doudoroff pathway			
20	6-Phosphogluconate dehydratase	sce8223	
21	KDPG aldolase	sce5154	*kdgA2*
Pyruvate metabolism			
22	Pyruvate carboxylase	sce3922	*accC1*
23	Phosphoenolpyruvate carboxylase	sce3427	*ppc*
24	Phosphoenolpyruvate carboxykinase	sce3007	*pckA1*
		sce4794	*pckA2*
		sce4201	*pckG*
25	Pyruvate dehydrogenase	sce1571	*pdhA*
		sce1570	*pdhB1*
		sce3801	*pdhB2*
		sce3800	*aceE*
26	Malic enzyme	sce5603	*maeB1*
		sce9116	*maeB2*

Gene numbers and gene names refer to the genome sequence [34]. The reaction numbers refer to the different biochemical reactions catalyzed in the metabolic network (Fig. 1).

regeneration of excess ATP or fine adjustment of metabolite levels [33]. For *S. cellulosum*, the exact metabolic function of this cycle remains to be elucidated.

NADPH Metabolism

On the basis of the determined fluxes, a detailed inspection of the NADPH metabolism of *S. cellulosum* was possible. *S. cellulosum* has an enormous anabolic requirement for NADPH of 23.5 mmol/g, mainly due to the high fraction of lipids present in cells (Table 1). With the biomass yield, an actual NADPH consumption flux of 156.8% results for *S. cellulosum*. Pathways supplying NADPH comprise glucose 6-phosphate dehydrogenase, 6-phosphogluconate dehydrogenase, and isocitrate dehydrogenase [38]. The

Table 4. Continued.

Reaction number	Gene product	Gene number	Gene name
TCA cycle			
27	Citrate synthase	sce1738	*cis1*
		sce8281	*cis2*
28	Aconitate hydratase	sce8137	*acnA*
29	Isocitrate dehydrogenase	sce6818	*icd2*
30	Oxoglutarate dehydrogenase	sce5670	*sucA*
31	Succinate-CoA ligase	sce9142	*sucC*
		sce9141	*sucD*
32	Succinate dehydrogenase	sce6554	*sdhA1*
		sce8303	*sdhA2*
		sce6555	*sdhB1*
		sce8309	*sdhB2*
		sce6553	*sdhC1*
		sce8307	*sdhC2*
33	Fumarate hydratase	sce9115	*fumC1*
		sce9130	*fumC2*
34	Malate dehydrogenase	sce1050	*mdh*
Glyoxylate cycle			
35	Isocitrate lyase	sce8725	*aceA*
36	Malate synthase	sce8726	*aceB*
Asparagine, threonine and glycine metabolism			
37	Asparagine synthase	sce3187	*asnB1*
		sce3826	*asnB2*
		sce8804	*asnB3*
		sce4939	*asnH*
38	Aspartate transaminase	sce4477	*aspB1*
		sce5648	*aspB2*
39[a]	Aspartate kinase	sce2535	*lysC1*
		sce6246	*lysC2*
	Aspartate-semialdehyde dehydrogenase	sce5347	*Asd*
	Homoserine dehydrogenase	sce4845	*Hom*
	Homoserine kinase	Adeh3331	
	Threonine synthase	sce9206	*thrC*
40	Threonine aldolase	sce2044	*ltaA*
41[a]	Phosphoglycerate dehydrogenase	sce4153	*serA1*
		sce5802	*serA2*
	Phosphoserine aminotransferase	sce4397	*serC*
	Phosphoserine phosphatase	sce0663	*serB*
		sce3610	*rsbX1*
		sce3741	*rsbX2*
42	Glycine hydroxymethyltransferase	sce6587	*glyA*

[a]Note that the different proteins involved in the biosynthesis from aspartate to threonine [39] and from 3PG to serine [41] are shown in the network figure as one lumped reaction step.

flux from these reactions adds up to a total NADPH supply of 215.8%. All together, NADPH supply and demand are about 60% higher than values reported for other prokaryotes such as *E. coli* [32], *B. subtilis* [8], or *C. glutamicum* [40]. Balancing the NADPH supplying and the NADPH consuming reactions results in an apparent excess of 60% for NADPH. This apparent imbalance indicates the *in vivo* activity of additional reactions acting as a sink for NADPH. A possible candidate for oxidation of NADPH is transhydrogenase annotated in the genome of So ce56. This enzyme catalyzes the interconversion of NADPH and NAD into NADP and NADH and vice versa and could be involved in *S. cellulosum* to balance the demand and supply of reduction equivalents [32]. The biosynthesis of secondary metabolites usually requires high amounts of NADPH. An effective supply of this reduction equivalent could therefore be an important driving force for the formation of such compounds in *S. cellulosum*.

Energy Metabolism

Based on the flux data, an estimate of the energy metabolism (*i.e.*, ATP formed and ATP utilized for growth and maintenance) in this slow-growing microorganism can be given. A total flux of 650% of reduction equivalents formed results from the flux data, when all NADH- and FADH-forming reactions are taken into account, and it is assumed that all NADPH not required for anabolism is converted into NADH and further directed into the respiratory chain. The ratio of ATP formed per electron channeled into the respiratory chain, (*i.e.*, the P/O ratio) in So ce56 is not exactly known, but likely is in the range of that of other microorganisms. Considering a P/O ratio of 1.5, recently determined for growth on minimal medium [27], leads to an ATP formation flux of 975%. Adding ATP, directly formed in glycolysis or indirectly formed as GTP in the TCA cycle, results in a total ATP formation flux of about 1,250%. The ATP production is thus much higher than the actual ATP demand for growth of 165%. The latter can be calculated from the biomass yield of 0.0531 g/mmol glucose (this

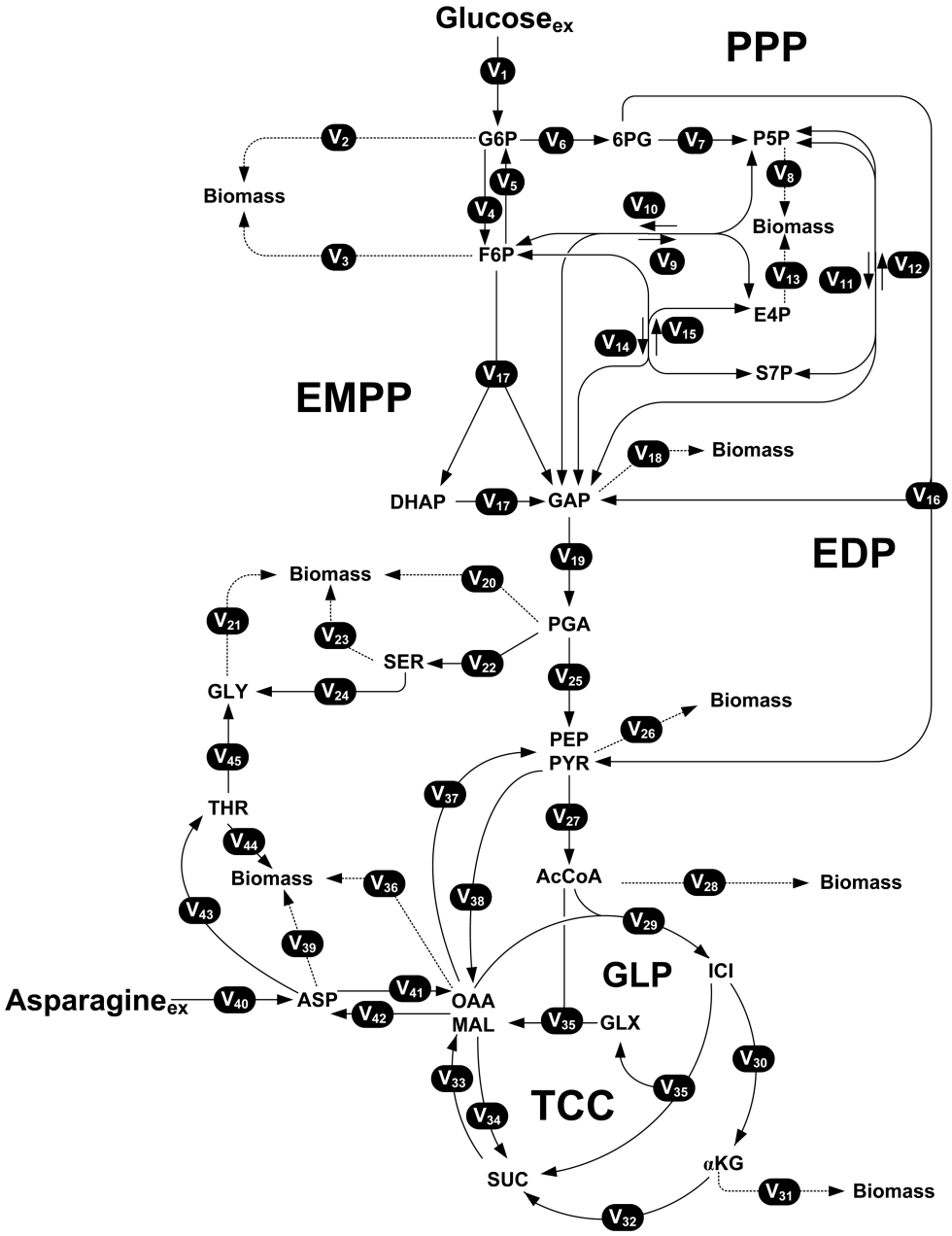

Fig. 4. Condensed metabolic network of the central metabolism of *Sorangium cellulosum* used for metabolic flux calculation. The reaction numbers refer to the metabolite mass balances given in the Appendix.

work) and the theoretical ATP demand of 31 mmol/g for the formation of bacterial cells [35]. This indicates that *S. cellulosum* utilizes only 10% of the ATP formed for growth whereas 90% is required for maintenance. A similar result is derived following the concept of cellular maintenance, originally introduced by Pirt [28], where the the total ATP demand is regarded as the sum of growth rate (μ) dependent requirement ($Y_{x/ATP}\cdot\mu$) and requirement for cellular maintenance (m_{ATP}), as given in Eq. (1).

$$r_{ATP}=Y_{X/ATP}\cdot\mu+m_{ATP} \quad (1)$$

Following this concept, the relative fraction of energy needed for maintenance is especially high in slow-growing organisms. Average experimental values for different microorganisms growing on minimal medium are $Y_{x/ATP}$=95.5 mmol ATP/g and m_{ATP}=13.2 mmol ATP/g·h [35]. Introducing these values and the specific growth rate of So ce56 (0.23 d^{-1}) into Eq. (1) suggests that about 90% of the energy formed in this organism is required for cellular maintenance. This agrees with the flux data given above. Although these calculations provide only a rough estimate, it is clear that the dominating fraction of energy in So ce56 is needed for maintenance. This could, to some extent, explain the apparent discrepancy between the relatively low biomass yield and the high flux through the energy-delivering TCA cycle.

Appendix

The following section provides details on the network model of So ce56. The calculations show that the network was overdetermined, so that a least-square approach was possible in the parameter estimation. The condensed network, as used for the flux estimation, was obtained from the annotated enzymes and pathways (Table 4) and is shown in Fig. 4. In total it comprises 45 fluxes. The pools of malate and oxaloacetate in the TCA cycle were lumped together. The same was performed for the pools of phosphoenolpyruvate and pyruvate in the glycolysis. As shown in Fig. 1, different enzymes can potentially catalyze fluxes between C_4 metabolites of the TCA cycle and C_3 metabolites from glycolysis. The tracer experiment of the present work cannot differentiate between the alternative anaplerotic reactions. The same holds for the possible gluconeogenic reactions. Therefore, the reactions of anaplerotic pyruvate carboxylation and of oxaloacetate decarboxylation in Fig. 4 represent the sum of the concerted action of all potential enzymes, respectively. Out of the 45 fluxes, 2 are directly accessible *via* quantification of the uptake of glucose (v_1) and asparagine (v_{40}). Taking biomass composition and measured biomass yield into account, a further 14 fluxes from anabolic precursors into biomass can be estimated. In addition, the following 18 metabolite balances can be formulated [Eqs. (2)–(19)].

Glucose 6-phosphate: $v_1-v_2-v_4+v_5-v_6=0$ (2)

Fructose 6-phosphate: $v_4-v_5-v_3+v_{10}-v_9+v_{15}-v_{14}-v_{17}=0$ (3)

6-Phosphogluconate: $v_6-v_7-v_{16}=0$ (4)

Pentose 5-phosphate: $v_7-v_8+v_9-v_{10}-2v_{11}+2v_{12}=0$ (5)

Erythrose 4-phosphate: $v_9-v_{10}-v_{13}+v_{15}-v_{14}=0$ (6)

Sedoheptulose 7-phosphate: $v_{11}-v_{12}+v_{14}-v_{15}=0$ (7)

Glyceraldehyde 3-phosphate: $2v_{17}+v_{10}-v_9+v_{14}-v_{15}+v_{11}-v_{12}+v_{16}-v_{18}-v_{19}=0$ (8)

3-Phosphoglycerate: $v_{19}-v_{20}-v_{22}-v_{25}=0$ (9)

PEP/pyruvate: $v_{25}-v_{26}-v_{27}+v_{37}-v_{38}+v_{16}=0$ (10)

Acetyl-CoA: $v_{27}-v_{28}-v_{29}-v_{35}=0$ (11)

Isocitrate: $v_{29}-v_{30}-v_{35}=0$ (12)

α-Ketoglutarate: $v_{30}-v_{31}-v_{32}=0$ (13)

Succinate: $v_{32}+v_{35}-v_{33}+v_{34}=0$ (14)

Oxaloacetate/malate: $v_{33}-v_{34}-v_{29}+v_{35}+v_{41}-v_{42}-v_{36}-v_{37}+v_{38}=0$ (15)

Aspartate: $v_{40}-v_{41}+v_{42}-v_{39}-v_{43}=0$ (16)

Threonine: $v_{43}-v_{44}-v_{45}=0$ (17)

Glycine: $v_{45}+v_{24}-v_{21}=0$ (18)

Serine: $v_{22}-v_{23}-v_{24}=0$ (19)

The rank of the corresponding stoichiometric matrix was calculated as 18, showing that all metabolite balances are linearly independent. Together with the 38 mass isotopomer fractions (Table 3), 72 informations were available. Thus, the network was overdetermined and the calculation of the entire number of 45 fluxes could be realized by a least-square approach.

References

1. Bacon, K., D. Clutter, R. H. Kottel, M. Orlowski, and D. White. 1975. Carbohydrate accumulation during myxospore formation in *Myxococcus xanthus*. *J. Bacteriol.* **124:** 1635–1636.
2. Becker, J., C. Klopprogge, O. Zelder, E. Heinzle, and C. Wittmann. 2005. Amplified expression of fructose 1,6-bisphosphatase in *Corynebacterium glutamicum* increases *in vivo* flux through the pentose phosphate pathway and lysine production on different carbon sources. *Appl. Environ. Microbiol.* **71:** 8587–8596.
3. Bligh, E. G. and W. J. Dyer. 1959. A rapid method of total lipid extraction and purification. *Can. J. Biochem. Physiol.* **37:** 911–917.

4. Bode, H. B. and R. Müller. 2006. Analysis of myxobacterial secondary metabolism goes molecular. *J. Ind. Microbiol. Biotechnol*. **33:** 577–588.
5. Bode, H. B., B. Zeggel, B. Silakowski, S. C. Wenzel, H. Reichenbach, and R. Müller. 2003. Steroid biosynthesis in prokaryotes: Identification of myxobacterial steroids and cloning of the first bacterial 2,3(*S*)-oxidosqualene cyclase from the myxobacterium *Stigmatella aurantiaca*. *Mol. Microbiol.* **47:** 471–481.
6. Bollag, D. M. 1997. Epothilones: Novel microtubule-stabilising agents. *Expert Opin. Investig. Drugs* **6:** 867–873.
7. Bollag, D. M., P. A. McQueney, J. Zhu, O. Hensens, L. Koupal, J. Liesch, M. Goetz, E. Lazarides, and C. M. Woods. 1995. Epothilones, a new class of microtubule-stabilizing agents with a taxol-like mechanism of action. *Cancer Res*. **55:** 2325–2333.
8. Dauner, M., J. E. Bailey, and U. Sauer. 2001. Metabolic flux analysis with a comprehensive isotopomer model in *Bacillus subtilis*. *Biotechnol. Bioeng.* **76:** 144–156.
9. Fischer, E. and U. Sauer. 2003. Metabolic flux profiling of *Escherichia coli* mutants in central carbon metabolism using GC-MS. *Eur. J. Biochem.* **270:** 880–891.
10. Frick, O. and C. Wittmann. 2005. Characterization of the metabolic shift between oxidative and fermentative growth in *Saccharomyces cerevisiae* by comparative 13C flux analysis. *Microb. Cell Fact.* **4:** 30.
11. Gerth, K., N. Bedorf, G. Höfle, H. Irschik, and H. Reichenbach. 1996. Epothilons A and B: Antifungal and cytotoxic compounds from *Sorangium cellulosum* (Myxobacteria). Production, physico-chemical and biological properties. *J. Antibiot. (Tokyo)* **49:** 560–563.
12. Gerth, K., N. Bedorf, H. Irschik, G. Höfle, and H. Reichenbach. 1994. The soraphens: A family of novel antifungal compounds from *Sorangium cellulosum* (Myxobacteria). I. Soraphen A1 alpha: Fermentation, isolation, biological properties. *J. Antibiot. (Tokyo)* **47:** 23–31.
13. Gerth, K., S. Pradella, O. Perlova, S. Beyer, and R. Müller. 2003. Myxobacteria: Proficient producers of novel natural products with various biological activities -- past and future biotechnological aspects with the focus on the genus *Sorangium*. *J. Biotechnol.* **106:** 233–253.
14. Gerth, K., D. Schummer, G. Höfle, H. Irschik, and H. Reichenbach. 1995. Ratjadon: A new antifungal compound from *Sorangium cellulosum* (myxobacteria)–production, physio-chemical and biological properties. *J. Antibiot. (Tokyo)* **48:** 973–976.
15. Gombert, A. K., M. Moreira dos Santos, B. Christensen, and J. Nielsen. 2001. Network identification and flux quantification in the central metabolism of *Saccharomyces cerevisiae* under different conditions of glucose repression. *J. Bacteriol.* **183:** 1441–1451.
16. Hardt, I. H., H. Steinmetz, K. Gerth, F. Sasse, H. Reichenbach, and G. Höfle. 2001. New natural epothilones from *Sorangium cellulosum*, strains So ce90/B2 and So ce90/D13: Isolation, structure elucidation, and SAR studies. *J. Nat. Prod.* **64:** 847–856.
17. Hofman, U. 1989. Physiologische Studien an *Sorangium cellulosum*, So ce 12. Technical University, Braunschweig.
18. Irschik, H., R. Jansen, K. Gerth, G. Höfle, and H. Reichenbach. 1995. Chivosazol A, a new inhibitor of eukaryotic organisms isolated from myxobacteria. *J. Antibiot. (Tokyo)* **48:** 962–966.
19. Irschik, H., R. Jansen, K. Gerth, G. Höfle, and H. Reichenbach. 1995. Disorazol A, an efficient inhibitor of eukaryotic organisms isolated from myxobacteria. *J. Antibiot. (Tokyo)* **48:** 31–35.
20. Irschik, H., R. Jansen, K. Gerth, G. Höfle, and H. Reichenbach. 1987. The sorangicins, novel and powerful inhibitors of eubacterial RNA polymerase isolated from myxobacteria. *J. Antibiot. (Tokyo)* **40:** 7–13.
21. Irschik, H., R. Jansen, K. Gerth, G. Höfle, and H. Reichenbach. 1995. Sorangiolid A, a new antibiotic isolated from the myxobacterium *Sorangium cellulosum* So ce 12. *J. Antibiot. (Tokyo)* **48:** 886–887.
22. Krömer, J. O., M. Fritz, E. Heinzle, and C. Wittmann. 2005. *In vivo* quantification of intracellular amino acids and intermediates of the methionine pathway in *Corynebacterium glutamicum*. *Anal. Biochem.* **340:** 171–173.
23. Krömer, J. O., O. Sorgenfrei, K. Klopprogge, E. Heinzle, and C. Wittmann. 2004. In-depth profiling of lysine-producing *Corynebacterium glutamicum* by combined analysis of the transcriptome, metabolome, and fluxome. *J. Bacteriol.* **186:** 1769–1784.
24. Lowry, O. H., N. J. Rosebrough, A. L. Farr, and R. J. Randall. 1951. Protein measurement with the Folin phenol reagent. *J. Biol. Chem*. **193:** 265–275.
25. Mahmud, T., H. B. Bode, B. Silakowski, R. M. Kroppenstedt, M. Xu, S. Nordhoff, G. Höfle, and R. Müller. 2002. A novel biosynthetic pathway providing precursors for fatty acid biosynthesis and secondary metabolite formation in myxobacteria. *J. Biol. Chem*. **277:** 32768–32774.
26. Minnikin, D. E., L. Alshamaony, and M. Goodfellow. 1975. Differentiation of *Mycobacterium*, *Nocardia*, and related taxa by thin-layer chromatographic analysis of whole-organism methanolysates. *J. Gen. Microbiol.* **88:** 200–204.
27. Noguchi, Y., Y. Nakai, N. Shimba, H. Toyosaki, Y. Kawahara, S. Sugimoto, and E. Suzuki. 2004. The energetic conversion competence of *Escherichia coli* during aerobic respiration studied by 31P NMR using a circulating fermentation system. *J. Biochem. (Tokyo)* **136:** 509–515.
28. Pirt, S. J. 1965. The maintenance energy of bacteria in growing cultures. *Proc. R. Soc. Lond. B Biol. Sci.* **163:** 224–231.
29. Pradella, S., A. Hans, C. Sproer, H. Reichenbach, K. Gerth, and S. Beyer. 2002. Characterisation, genome size and genetic manipulation of the myxobacterium *Sorangium cellulosum* So ce56. *Arch. Microbiol.* **178:** 484–492.
30. Reichenbach, H. 2001. Myxobacteria, producers of novel bioactive substances. *J. Ind. Microbiol. Biotechnol.* **27:** 149–156.
31. Reichenbach, H. 1986. The myxobacteria: Common organisms with uncommon behaviour. *Microbiol. Sci.* **3:** 268–274.
32. Sauer, U., F. Canonaco, S. Heri, A. Perrenoud, and E. Fischer. 2004. The soluble and membrane-bound transhydrogenases UdhA and PntAB have divergent functions in NADPH metabolism of *Escherichia coli*. *J. Biol. Chem*. **279:** 6613–6619.
33. Sauer, U. and B. J. Eikmanns. 2005. The PEP-pyruvate-oxaloacetate node as the switch point for carbon flux distribution in bacteria. *FEMS Microbiol. Rev.* **29:** 765–794.
34. Schneiker, S., O. Perlova, A. Alici, M. O. Altmeyer, D. Bartels, T. Bekel, *et al*. 2007. Complete sequence of the largest known

bacterial genome from the myxobacterium *Sorangium cellulosum*. *Nat. Biotechnol.* **25:** 1281–1289.
35. Stouthamer, A. H. 1979. The search for correlation between theoretical and experimental growth yields, pp. 1–47. *In* J. R. Quayle (ed.), *Microbial Biochemistry*, Vol. 21. University Park Press, Baltimore.
36. Thomas, E., J. Tabernero, M. Fornier, P. Conte, P. Fumoleau, A. Lluch, *et al.* 2007. Phase II clinical trial of ixabepilone (BMS-247550), an epothilone B analog, in patients with taxane-resistant metastatic breast cancer. *J. Clin. Oncol.* **25:** 3399–3406.
37. van Winden, W. A., C. Wittmann, E. Heinzle, and J. J. Heijnen. 2002. Correcting mass isotopomer distributions for naturally occurring isotopes. *Biotechnol. Bioeng.* **80:** 477–479.
38. Watson, B. F. and M. Dworkin. 1968. Comparative intermediary metabolism of vegetative cells and microcysts of *Myxococcus xanthus*. *J. Bacteriol.* **96:** 1465–1473.
39. Wittmann, C. 2002. Metabolic flux analysis using mass spectrometry. *Adv. Biochem. Eng. Biotechnol.* **74:** 39–64.
40. Wittmann, C. and A. de Graaf. 2005. Metabolic flux analysis in *Corynebacterium glutamicum*, pp. 277–304. *In* L. Eggeling and M. Bott (eds.), *Handbook of Corynebacterium glutamicum*. CRC Press, Boca Raton.
41. Wittmann, C., M. Hans, and E. Heinzle. 2002. *In vivo* analysis of intracellular amino acid labelings by GC/MS. *Anal. Biochem.* **307:** 379–382.
42. Wittmann, C. and E. Heinzle. 2002. Genealogy profiling through strain improvement by using metabolic network analysis: Metabolic flux genealogy of several generations of lysine-producing corynebacteria. *Appl. Environ. Microbiol.* **68:** 5843–5859.
43. Wittmann, C. and E. Heinzle. 1999. Mass spectrometry for metabolic flux analysis. *Biotechnol. Bioeng.* **62:** 739–750.
44. Wittmann, C. and E. Heinzle. 2001. Modeling and experimental design for metabolic flux analysis of lysine-producing Corynebacteria by mass spectrometry. *Metab. Eng.* **3:** 173–191.
45. Wittmann, C., P. Kiefer, and O. Zelder. 2004. Metabolic fluxes in *Corynebacterium glutamicum* during lysine production with sucrose as carbon source. *Appl. Environ. Microbiol.* **70:** 7277–7287.
46. Wittmann, C., H. M. Kim, and E. Heinzle. 2004. Metabolic network analysis of lysine producing *Corynebacterium glutamicum* at a miniaturized scale. *Biotechnol. Bioeng.* **87:** 1–6.
47. Wittmann, C., H. M. Kim, G. John, and E. Heinzle. 2003. Characterization and application of an optical sensor for quantification of dissolved O_2 in shake-flasks. *Biotechnol. Lett.* **25:** 377–380.